IMPT: Beam Scanning

Simulations of scanning with
various beam shapes

W. Jennekens

Northeast Proton Therapy Center
Report Number NPTC-5200

March 2003

Eindhoven University of Technology
Faculty of Applied Physics
Department of Medical Physics

IMPT: beam scanning

Simulations of scanning with various beam shapes

W. Jennekens

March 2003

Internship Report
Supervisors: ir. H.J. van Kleffens (TU/e)
Prof. dr. T.R. Bortfeld (MGH, NPTC)

Abstract

The goal of this study was to investigate the possibilities of intensity modulated proton beam scanning with the current patient treatment setup at the Northeast Proton Therapy Center, the proton radiation oncology facility of the Massachusetts General Hospital in Boston, USA. This was investigated by simulating irradiation with various beam profiles resulting from the use of apertures, instead of quadrupole magnets, to narrow and sharpen the proton beam profiles. From these simulations, it follows that it's possible to use broad beams in combination with an aperture to deliver dose distributions comparable to those delivered with a narrow Gaussian beam, but this method has certain disadvantages. Because of the required small aperture diameter, a large part of the beam intensity is lost, reducing efficiency substantially. This also results in the additional production of neutrons due to interaction of the protons with aperture material. Furthermore, the optimal width of the aperture depends on the shape of the desired dose distribution.

The model developed for this study was also used to investigate the effects of tumor motion on the dose conformality, and the possibilities of compensating for these at the treatment planning stage. Motion compensation was accomplished by including the tumor position probability distribution, the so-called motion kernel, in the optimization process. By convolving the beam profile with this motion kernel, the frame of reference was changed from beam to tumor. Subsequently optimizing the intensity distribution for this effective beam profile accounts for the tumor motion. A simulation using sinusoidal tumor motion, and a uniform dose prescription, showed that the effect of tumor motion may be reduced significantly if the dose is optimized using the motion kernel. The disadvantage of this method is that, since an averaged motion kernel is used, irregularities in tumor motion will produce additional errors, which should be studied as well.

Contents

1 Introduction **1**

2 Theory **3**
2.1 Multiple Coulomb scattering 3
2.2 Newton gradient algorithm 3

3 Model **5**
3.1 Beam profiles 5
3.2 Optimization 6
3.3 Motion kernel 8

4 Simulations **10**
4.1 Uniform dose distribution 10
4.2 Smooth dose distribution 11
4.3 Clinical case 11
4.4 Motion compensation 12

5 Results **15**
5.1 Uniform dose distribution 15
5.2 Smooth dose distribution 16
5.3 Clinical case 17
5.4 Motion compensation 18

6 Discussion **30**
6.1 Apertures 30
6.2 Motion compensation 31

7 Conclusions **32**
7.1 Apertures 32
7.2 Motion compensation 32
7.3 Outlook 33

Bibliography **34**

A Motion kernel **35**

B Tikhonov optimization **36**

Chapter 1

Introduction

In radiation therapy, i.e. the treatment of cancer tumors with radiation, the ultimate goal is to deliver a high, uniform dose to the tumor volume while completely sparing the surrounding healthy tissue. In practice however, this is not achievable. There will always be irradiation of normal tissue and non-uniformity of tumor dose. The extent to which the delivered high dose volume conforms to the tumor volume depends both on the radiation source, e.g. photons or protons, and the way the tumor is irradiated [Lom99].

Massachusetts General Hospital (MGH), located in Boston, uses both photon and proton radiation to treat patients. Photon beams are characterized by depth-dose distributions having an exponential decay, while clinical proton beams are characterized by depth-dose distributions having a relatively uniform low-dose entrance region, followed by a region of high dose at the tumor, the Bragg peak, then a steep fall-off to virtually zero dose. Typical depth-dose distributions for clinical photon and proton beams can be seen in figure 1.1. Because of the high degree of dose localization, proton may have superior dose distributions compared to photons in comparable beam configurations. Moreover, due to the steep fall-off, proton beams can be aimed directly at critical structures lying beyond the target. A disadvantage of proton beams is that, although the dose is localized, due to scattering the penumbra is usually not as sharp as with photons. The latest development in proton therapy is pencil beam scanning, which has been done at PSI (Paul Scherrer Institut, Villingen, Switzerland) and GSI (Gesellschaft für Schwerionenforschung mbH, Darmstadt, Germany), and is currently under development at MGH. Here, instead of using a large uniform field and patient specific compensators, a narrow proton beam is scanned over the tumor volume. The amount of dose deposited at a certain point is controlled by dynamically adjusting the beam intensity and/or scanning speed, while the range of the beam is controlled by adjusting proton energy (either directly at the accelerator or through a range modulator). The advantages of scanning are that (a) it has the potential to construct dose distributions with complex shapes, nonhomogeneous if desired, and high conformation; (b) patient specific hardware is no longer needed; (c) all protons transported in the beam line are used in the patient and (d) because scattering systems are no longer needed, compact gantries can be designed [Ped95]. To prepare the current patient treatment setup at MGH for pencil beam scanning, patient treatment would have to be postponed for a period of

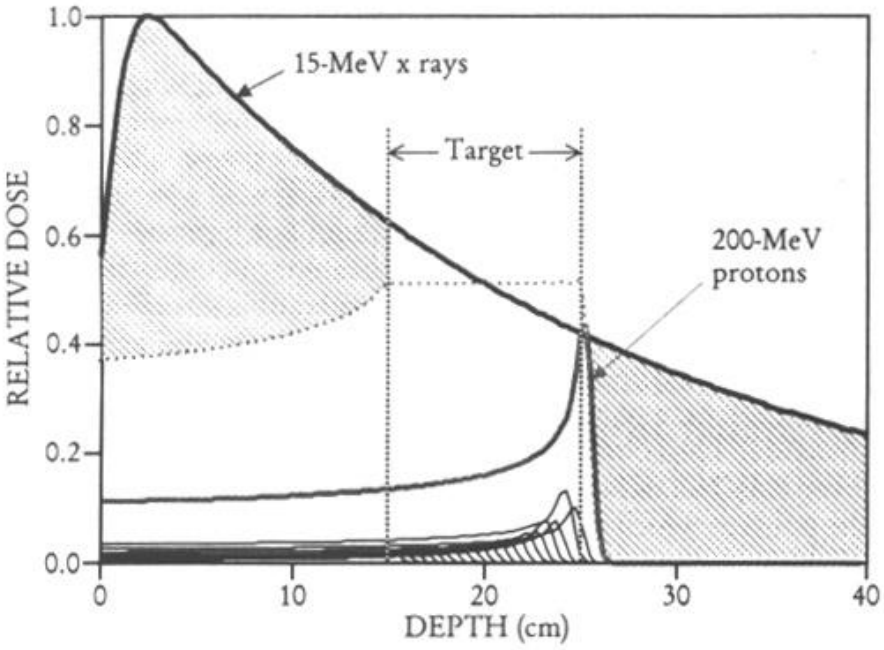

Figure 1.1: Typical depth-dose distributions for clinical photon and proton beams [Boy02].

up to four months in order to install and test all the new equipment.

The goal of this study is to investigate the possibilities of pencil beam scanning using the current patient treatment setup, with as few modifications as possible. This has been done through simulations using a computer model in Matlab. Furthermore, the abilities of the model have also been used to investigate the effects of tumor motion (e.g. due to breathing) on the delivered dose conformality, and the possibilities to compensate for these at the treatment planning stage. Chapter 2 presents a brief overview of physical and mathematical theory used in this study. The model used for simulations is described in chapter 3. Chapter 4 outlines the simulation plans. The results of these simulations are presented in chapter 5. In chapter 6 the results are discussed and final conclusions are given in chapter 7.

Chapter 2

Theory

In this chapter, the physical and mathematical theory and concepts used in this study are explained. Section 2.1 describes the scattering of proton beams in a medium. The optimization algorithm used in the simulation model is described in section 2.2.

2.1 Multiple Coulomb scattering

Charged particles travelling through a medium are deflected by many small-angle scatters. Most of these deflections are due to Coulomb scattering from nuclei, and hence the effect is called multiple Coulomb scattering. As a result of multiple Coulomb scattering (e.g. in human tissue), an ideal, infinitesimally narrow, pencil beam will acquire a nearly Gaussian profile at the Bragg peak. For scattering in human tissue the width σ_{scat} of this Gaussian profile is approximately

$$\sigma_{\text{scat}} \approx 0.02 \cdot d, \tag{2.1}$$

where d is the radiological tissue penetration depth.

For non-infinitesimally narrow beams with initial pre-scattering beam width σ_{in}, the effective beam width σ_{eff} is given by

$$\sigma_{\text{eff}}(d) = \sqrt{\sigma_{\text{in}}^2 + \sigma_{\text{scat}}^2(d)}. \tag{2.2}$$

2.2 Newton gradient algorithm

The main optimization algorithm used in this study is a (modified) Newton Gradient approach. Newton's method requires the error surface to be quadratic, and it's effectiveness is directly tied to the accuracy of this assumption. For most problems, the error surface can be well approximated by a quadratic form near the solution. The idea in Newton's method is to minimize at each iteration the quadratic approximation of a function g around the current point x^k given by

$$g^k(x) = g(x^k) + \nabla g(x^k)^T (x - x^k) + \frac{1}{2}(x - x^k)^T \nabla^2 g(x^k)(x - x^k). \tag{2.3}$$

By setting the derivative of $g^k(x)$ to zero,

$$\nabla g(x^k) + \nabla^2 g(x^k)(x - x^k) = 0, \tag{2.4}$$

we obtain the next iterate x^{k+1} as the minimum of $g^k(x)$:

$$x^{k+1} = x^k - (\nabla^2 g(x^k))^{-1} \nabla g(x^k). \tag{2.5}$$

This is the pure Newton iteration. It corresponds to the more general iteration

$$x^{k+1} = x^k - \alpha^k (\nabla^2 g(x^k))^{-1} \nabla g(x^k), \tag{2.6}$$

where the step size $\alpha^k = 1$. Newton's method typically converges very fast asymptotically.

Chapter 3

Model

This chapter describes the model developed and used for this study. This model calculates the optimal intensity profile for a given prescription dose by iteratively updating beam weights at every (discretized) position until the resulting dose distribution satisfies a certain criterium. The optimal intensity profile can be calculated for different beam profiles, described in section 3.1. For simplicity, the profiles used in this study are one dimensional.

3.1 Beam profiles

A proton beam profile gives the energy deposited by this beam per unit of mass at a certain position, for unity proton flux. This profile is evaluated at the Bragg peak, in the direction perpendicular to the beam. The various beam profiles used in this study are described in the following sections.

3.1.1 Gaussian

The main beam profile used in this study is a Gaussian profile, given by

$$B(x) = C \exp(-\frac{x^2}{2\sigma^2}), \tag{3.1}$$

with B the beam intensity at a certain position x, C a normalization constant and σ the width of the profile. The current nozzle can deliver proton beams with a width of $\sigma = 8$ mm at the patient's skin surface. A new nozzle, currently being designed and tested, will be able to deliver beams with a width of $\sigma = 3$ mm. This nozzle uses quadrupole magnets to focus the proton beam. Both the 3 mm and the 8 mm Gaussian profiles are plotted in figure 3.1.

3.1.2 Cut-off Gaussian

To obtain this beam profile, Gaussian profile (3.1) with $\sigma = 8$ mm is cut off using a window filter. The width of this filter is defined as the aperture opening. Because the aperture used

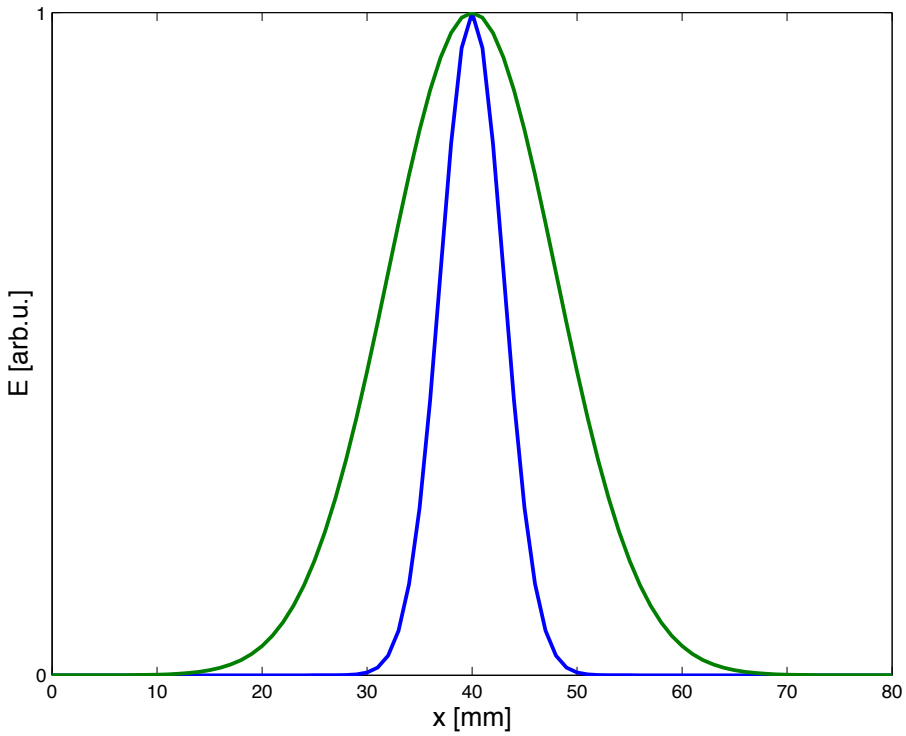

Figure 3.1: Gaussian proton beam profiles, with widths of $\sigma = 8$ mm (green), the minimum beam width currently attainable at the NPTC, and $\sigma = 3$ mm (blue), the beam width attainable with a new nozzle.

to obtain this profile would be placed upstream from the nozzle, the beam would travel through air for a certain distance. Due to multiple Coulomb scattering in air, the beam would have less sharp edges at the patient's skin surface. To account for this scattering, the remaining profile is convolved with a narrow Gaussian, with $\sigma = 0.9$ mm.

3.2 Optimization

3.2.1 Newton Gradient algorithm

The dose d_i for any voxel i is given by

$$d_i = \sum_{i=1}^{N_j} D_{ij} w_j, \tag{3.2}$$

where D_{ij} is the dose matrix, i.e. the dose delivered to voxel i by beam element j, and w_j the weight of beam element j [Nil01]. Equation (3.2) describes the convolution of beam profile and intensity distribution. Using a generalized objective function, the derivatives

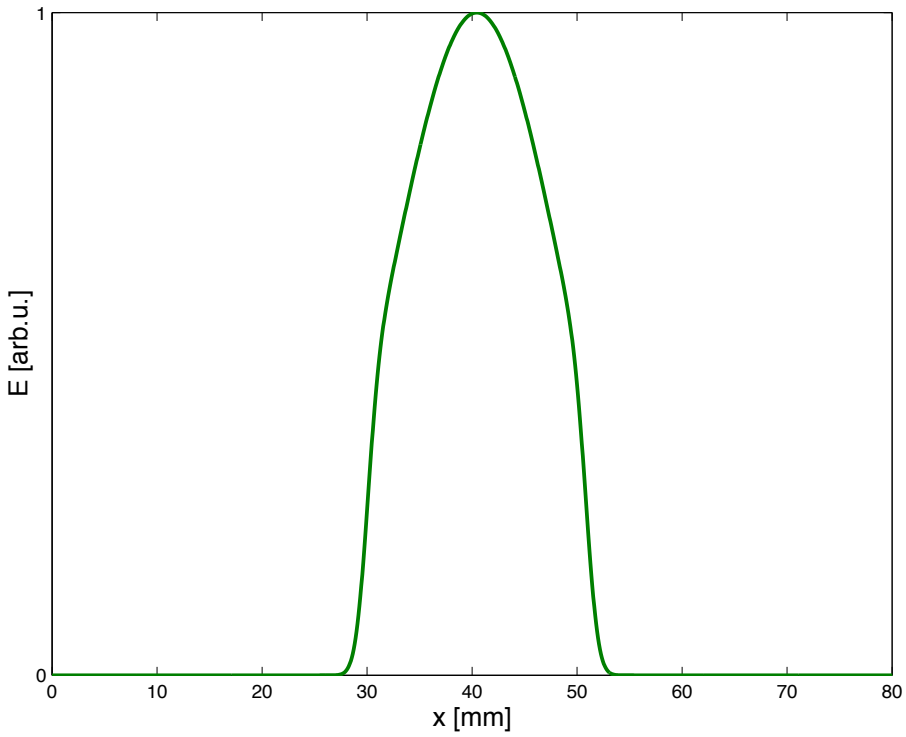

Figure 3.2: Gaussian proton beam profile, cut off by an aperture to get a relatively steep fall-off and convolved with a narrow Gaussian to simulate Multiple Coulomb scattering

of the function for the voxel i with penalty factor s_i and prescribed dose d^{pres} can then be calculated by

$$F_t = \sum_i^{N_t} s_u^t [d_t^{\text{pres}} - d_i]_+^2 + s_o^t [d_i - d_t^{\text{pres}}]_+^2, \tag{3.3}$$

with s_u^t and s_o^t penalty factors for respectively underdosage and overdosage in the target region and $[x]_+$ a positivity filter, defined by

$$[x]_+ = xH(x) = \begin{cases} x & : \quad x \geq 0 \\ 0 & : \quad \text{else} \end{cases} \tag{3.4}$$

For the organs at risk (AOR) (r), another objective function is defined:

$$F_r = \sum_i^{N_r} s_o^r [d_i - d_r^{\max}]_+^2, \tag{3.5}$$

where $d_r^{\max}$ is the maximum dose which is allowed for the organ at risk r. The penalty for overdosage is given by s_o^r and N_r is the number of voxels which belong to organ r.

The total objective function is then given by summation of the individual objective functions for all targets and organs-at-risk, according to

$$F = \sum_{t}^{N^{\text{target}}} F_t + \sum_{r}^{N^{\text{organs}}} F_r. \tag{3.6}$$

By using the Newton gradient approach the result for the weights is then

$$w_j^{t+1} = \left[w_j^t - \alpha \frac{\frac{dF}{dw_j}}{\frac{d^2F}{dw_j^2}} \right]_+, \tag{3.7}$$

with α as a normalization factor. The result of this calculation is a procedure describing how to update the weights in every iteration step:

$$w_j^{t+1} = \left[w_j^t - \alpha \frac{\sum_i 2 s_i [d_i - d_i^{\text{pres}}] D_{ij}}{2 \sum_i s_i D_{ij}^2} \right]_+, \tag{3.8}$$

3.3 Motion kernel

The ability to use different beam shapes in the model has also been used to investigate the effects of tumor motion (e.g. due to breathing) and the possibilities of compensating for these in the treatment planning stage. To accomplish this, the motion of the tumor was first transferred to the beam (i.e. changing the frame of reference from beam to target) by convolving the beam kernel with a motion kernel. This is possible because the time necessary for a single scan ($\sim 0.5\ s$) is much smaller than the length of the breathing cycle, and the total treatment time (several scans per fraction, over 20-30 fractions) is much larger than the period of motion. Assuming no deformation, the target thus has a certain position probability density distribution. This distribution is called the motion kernel. The motion may be approximated as sinusoidal and the kernel shape [appendix A] is then given by

$$M(\xi) \sim \frac{1}{\sqrt{1-\xi^2}}, \quad |\xi| < 1, \tag{3.9}$$

where M is the probability of finding the target at a certain position and ξ is the normalized target position, i.e. the position divided by the maximum displacement. The kernel can be seen in figure 3.3. The integral of the kernel over the full range should be equal to unity, because the sum of all probabilities is always one. The effective beam kernel is given by

$$B_{\text{eff}} = M \otimes B, \tag{3.10}$$

the convolution of the motion kernel and the beam kernel, and motion compensation is then accomplished by optimizing the intensity distribution for this effective beam and thus taking the position probability density distribution into account.

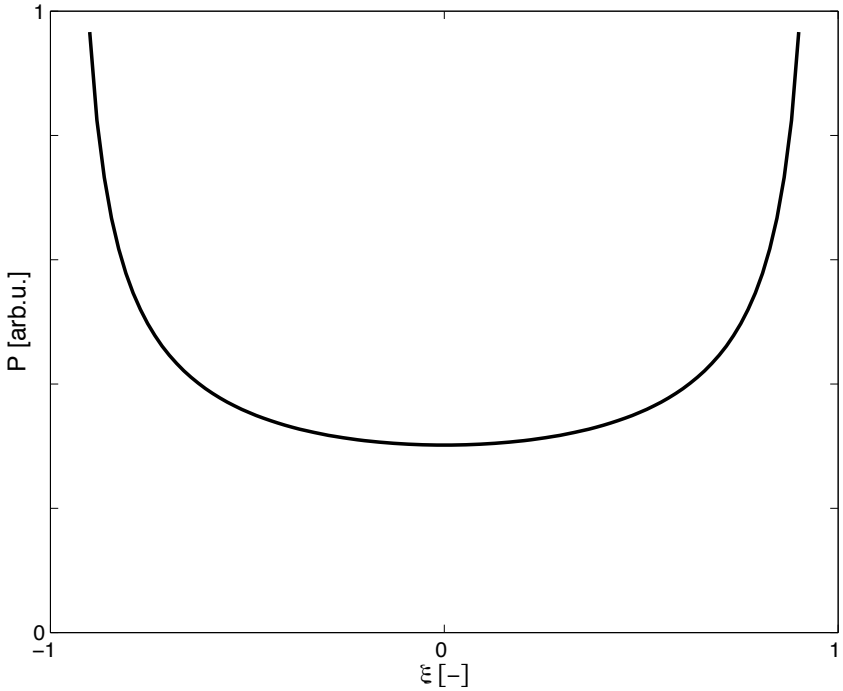

Figure 3.3: Motion kernel, represents the probability to find the target at a certain normalized position ξ assuming a sinusoidal motion.

Chapter 4

Simulations

The main goal of this study was to investigate whether a broad Gaussian beam, cut off using an aperture, can deliver dose distributions comparable to those delivered with a Gaussian beam of $\sigma = 3$ mm. To accomplish this, the optimal intensity distribution has been calculated for different prescription doses and different aperture widths. The doses corresponding to these intensity distributions have been compared to the dose delivery of a 3 mm Gaussian beam. The calculation of the intensity distributions has been done using the optimization algorithm described in section 3.2, with a discretization of 1 mm. The optimization routine was stopped when the relative objective function decrease was less than 0.1%. These calculations are described in sections 4.1 through 4.3. The second part of this study was to investigate the effects of tumor motion on the dose conformality, and the possibilities of compensating for these in the treatment planning stage. The simulations done in order to accomplish this are described in section 4.4.

4.1 Uniform dose distribution

To investigate the possibilities of delivering dose distributions with steep edges, a block shaped prescribed dose distribution, with a uniform dose delivered to the target and no dose outside the target, has been used to generate intensity distributions. This dose distribution is an idealized case, since it's impossible to avoid giving dose to surrounding tissue while uniformly irradiating a target. The prescription dose $D(x)$ is given by

$$D(x) = C(H(x) - H(x - a)), \tag{4.1}$$

with $H(x)$ a Heavyside (or step-) function, C a constant defining the dose and a a constant defining the width of the block. This dose profile is shown in figure 4.1. Simulations have been done with $a = 300$ mm and $a = 30$ mm. The prescription dose was kept constant at $C = 50$ Gy. All simulations in this study have been done with all penalty factors set to unity ($w = 1$). Because of this, the objective function value is equal to χ^2.

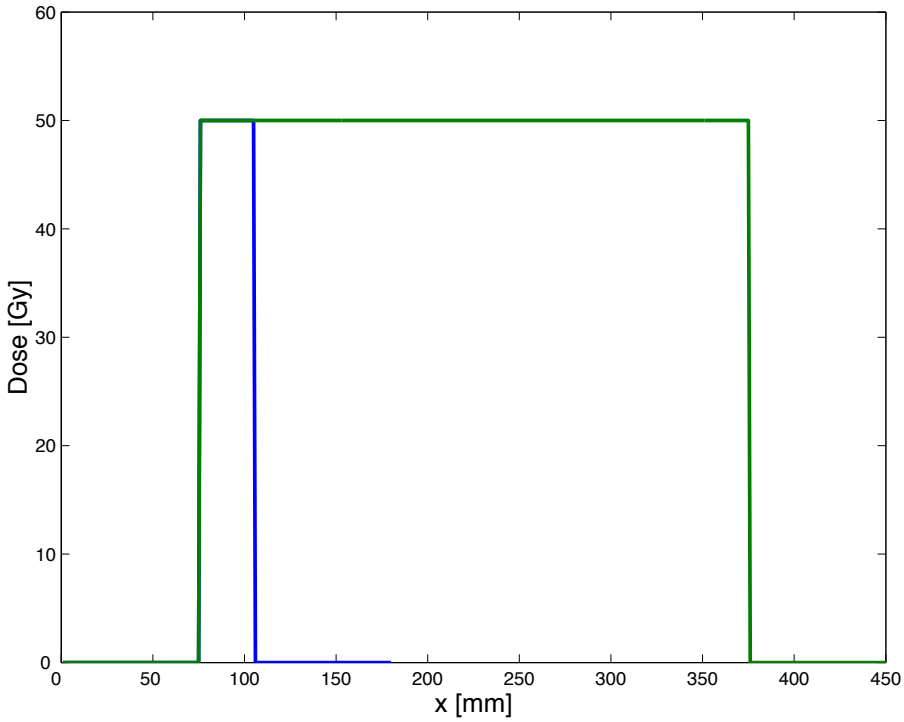

Figure 4.1: Uniform, block shaped, prescription dose profiles with widths of 30 mm (blue) and 300 mm (green) used in simulations.

4.2 Smooth dose distribution

Because a step function can never be achieved using a beam of finite width, a prescribed dose with a larger penumbra has also been used. In these simulations, the prescribed dose is the dose delivered by a Gaussian beam with $\sigma = 3$ mm using a constant intensity over a certain width. The intensity profile for this prescription dose is given by

$$I(x) = F(H(x) - H(x - a)), \tag{4.2}$$

where F is a constant defining the intensity. The dose prescription is thus given by

$$D(x) = B_{3\text{mm}}(x) \otimes I(x), \tag{4.3}$$

the convolution of a 3 mm Gaussian beam with the intensity profile, and is shown in figure 4.2. This simulation has been done for $a = 30$ mm, with a dose of 50 Gy.

4.3 Clinical case

Finally, to simulate a clinical case, a dose distribution calculated by treatment planning system Konrad has been used as input. This plan was generated for treatment of a Chordoma of the Sacrum, and consists of three proton fields, at angles of 300°, 0° and 60°.

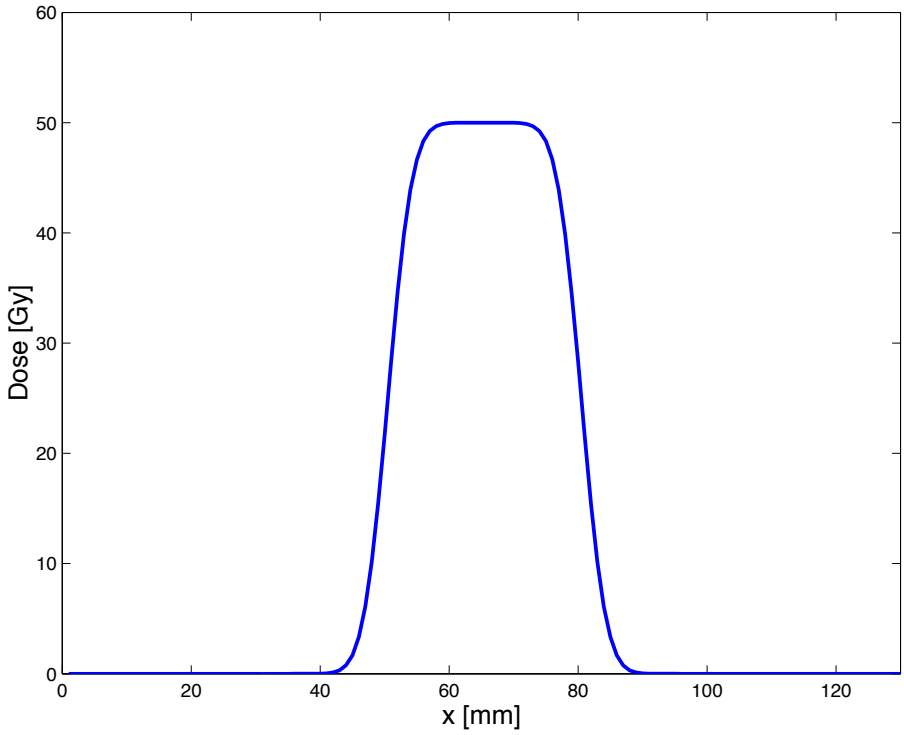

Figure 4.2: Smooth prescription dose used in simulations. This dose is generated by scanning a Gaussian beam with $\sigma = 3$ mm over a width of 30mm using a constant intensity. The dose distribution is scaled to 50 Gy.

The target dose was 75 Gy. The generated dose distribution can be seen in figure 4.3. A one-dimensional dose profile delivered along a single scanning line by the 0° field was chosen as input for the simulations. The scanning of this line was done in the y-direction, at $x = 20$ mm. This dose prescription can be seen in figure 4.4.

4.4 Motion compensation

To investigate to which degree it is possible to compensate for tumor motion in the treatment planning stage, when this motion is exactly known, a simulation of dose delivery has been done with and without motion compensation according to the principle described in section 3.3. The dose prescription used for these simulations was an ideal, block shaped, dose distribution, according to equation (4.1). The proton beam used in these simulations was a Gaussian beam with $\sigma = 3$ mm.

Aforementioned simulations give intensity profiles that are optimized for the given prescribed dose distribution 1) assuming a static target (Gaussian beam kernel) and 2) compensated for target motion (Gaussian beam kernel convolved with the motion kernel). By convolving the resulting intensity profiles with a Gaussian, the dose distributions that

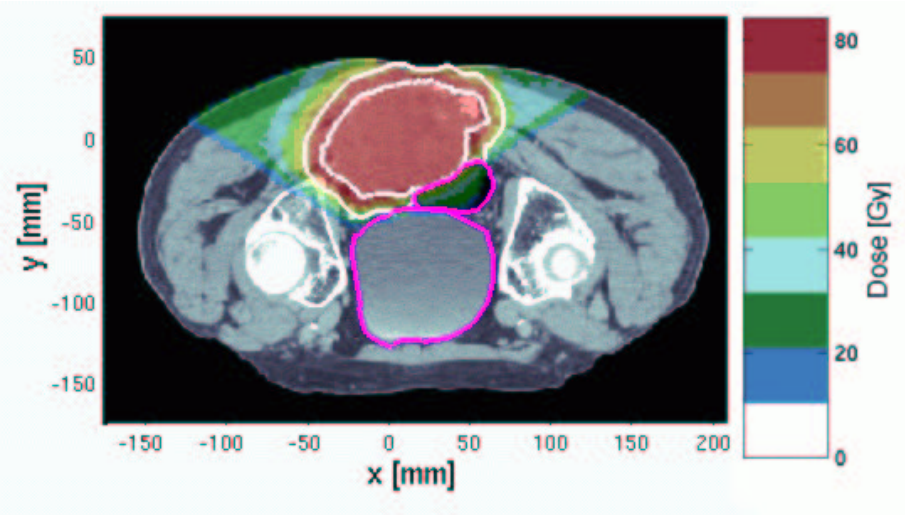

Figure 4.3: Treatment plan for a Chordoma of the Sacrum, generated by KonRad. The plan consists of three proton fields at angles of 300°, 0° and 60° and was calculated for a target dose of 75 Gy. Outlined in the CT image are Clinical Target Volume (CTV, inner, white), Planning Target Volume (PTV, outer, white), rectum (top, pink) and the bladder (bottom, pink).

would be delivered to a static target can be found. Convolving these dose distributions with the motion kernel gives the dose distributions that would be delivered to a moving target.

In these simulations, the optimal dose profile (i.e. the intensity profile optimized for a static target, convolved with a Gaussian beam kernel) is compared to the compensated and the non-compensated dose distributions to a moving target. The non-compensated distribution was calculated by convolving the optimal dose profile with the motion kernel.

Also calculated is the dose distribution that, when convolved with the motion kernel, gives the compensated dose distribution to the moving target. It may be obtained by convolving the intensity profile resulting from the compensated optimization with only a Gaussian kernel. This is the dose distribution that would be delivered to a static phantom, using the motion-compensated (i.e. optimized for the case of a moving target) intensity map and agrees with the compensated distribution delivered to a moving target, if the motion kernel describes the actual motion correctly.

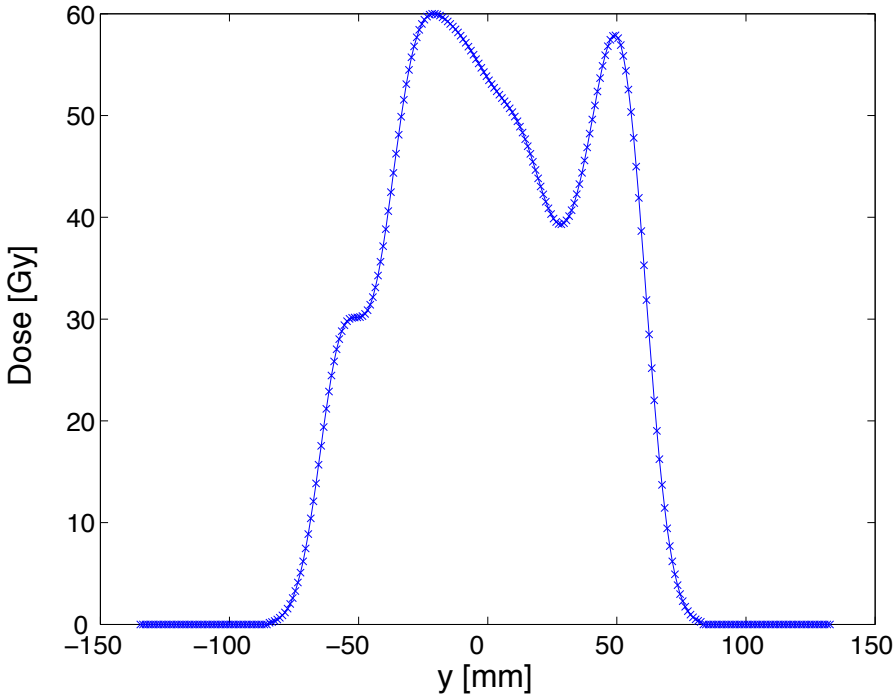

Figure 4.4: Prescription dose for Chordoma of the Sacrum, 0° field, scanned in y-direction at $x = 20$ mm.

Chapter 5

Results

5.1 Uniform dose distribution

From the results of the simulation using a uniform prescription dose distribution, with a width of 300 mm and a Gaussian beam with $\sigma = 3$ mm, shown in figure 5.1, it can be seen that, with a certain amount of intensity modulation, a reasonable approximation of the block shaped prescription dose distribution can be achieved. The same simulation has also been done using a Gaussian beam with $\sigma = 8$ mm, the result of which can be seen in figure 5.2. The intensity distribution in this figure (top plot) shows that, compared to the 3 mm beam, the use of the 8 mm beam results in an increased modulation period in the intensity profile. This is due to the increased beam profile width. Furthermore, it can be seen that the resulting dose distribution is an inferior approximation of the prescription dose profile compared to the dose distribution shown in figure 5.1. A better approximation can be achieved by using an aperture, to be seen in figure 5.3. This figure shows the required intensity distribution fluctuates strongly. This high modulation is caused by the decreased overlap from neighboring beam elements, as a result of the decreased beam profile penumbra. Also, the modulation period has decreased compared to figure 5.2. This is due to the decreased beam profile width, resulting from the use of an aperture.

The results of all simulations using a prescription dose profile width of 300 mm and different aperture widths have been summarized in figure 5.4. As can be seen from this figure, it's possible to reach similar objective function values using a cut off Gaussian beam as when using a narrow Gaussian beam. To accomplish this, the aperture diameter would have to be about 15 mm, resulting in an intensity loss of about 64% for the 8 mm beam.

For the simulations with a =30 mm, summarized in figure 5.5, it shows that modulations are visible when plotting χ^2 as function of the aperture width. These modulations are due to interference between intensity modulations from the left and the right side of the intensity distribution. This can be seen by comparing the intensity distribution at the first minimum in χ^2, which is for an aperture diameter of 17 mm, to the intensity distribution at the first maximum, which occurs with an aperture diameter of 13 mm and the intensity distribution at the second minimum, which is for an aperture diameter of 11 mm. At the

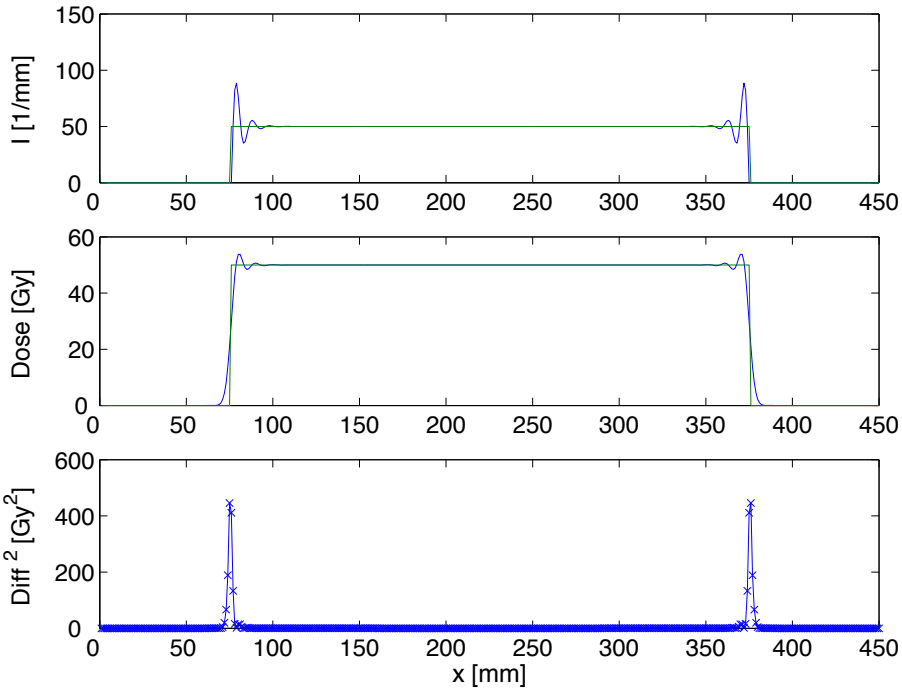

Figure 5.1: Results of a simulation for a block shaped prescription dose profile, with $a = 300$ mm and a Gaussian beam with $\sigma = 3$ mm. Top graph shows intensity (blue) as function of position. First intensity estimate for the iterations is also plotted (green). Center graph shows calculated dose (blue) and prescription dose (green) as function of position. Bottom graph shows squared difference between calculated and prescribed dose.

first minimum, to be seen in figure 5.6, there are two peaks in the intensity distribution. At the first maximum, figure 5.7, a third peak appears in the middle, but doesn't fit exactly in between. There is also a rise in amplitude at the edges of the distribution. At the second minimum, figure 5.8, there are three clear peaks in intensity. Because of the decreased beam profile width, all three peaks fit inside the distribution. Apparently there is a minimum in χ^2 when an integer number of modulation periods fits inside the intensity distribution. Because the intensity modulations decrease in amplitude towards the middle of the target, this effect decreases for increasing prescription dose widths.

5.2 Smooth dose distribution

The results of simulations using a smooth prescription dose profile and different aperture widths are summarized in figure 5.9, showing χ^2 as function of aperture width. From this figure, it can be seen that the prescription dose profile can be very well approximated using a broad Gaussian beam and an aperture. The modulations in χ^2 are still visible.

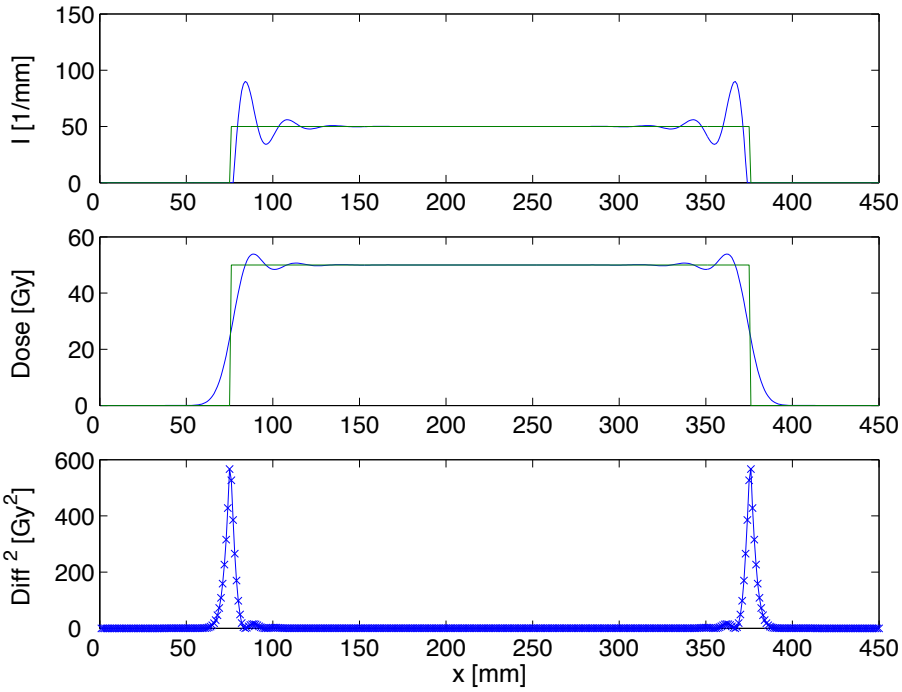

Figure 5.2: Results of a simulation for a block shaped prescription dose profile, with $a = 300$ mm and a Gaussian beam with $\sigma = 8$ mm. Top graph shows intensity (blue) as function of position. First intensity estimate for the iterations is also plotted (green). Center graph shows calculated dose (blue) and prescription dose (green) as function of position. Bottom graph shows squared difference between calculated and prescribed dose.

The optimal results at the first modulation minimum, i.e. for an aperture width of 17 mm, are shown in figure 5.10. It can be seen that, to obtain a result similar to the dose generated by the 3 mm Gaussian beam with constant intensity map, a considerable amount of intensity modulation is still required.

5.3 Clinical case

Figure 5.11 shows the optimal intensity distribution, dose distribution and the square of the local difference between the prescribed dose and calculated dose for a Gaussian beam with $\sigma = 3$ mm. From this figure, it can be seen that the prescription dose profile can be approximated very well and that the intensity distribution has a profile similar to the dose prescription distribution, which was used as an initial intensity guess.

The results for the same simulation using a Gaussian beam with $\sigma = 8$ mm are shown in figure 5.12. From this figure it can be seen that it's also possible to approximate the prescription dose profile very well using beam with $\sigma = 8$ mm, but the intensity

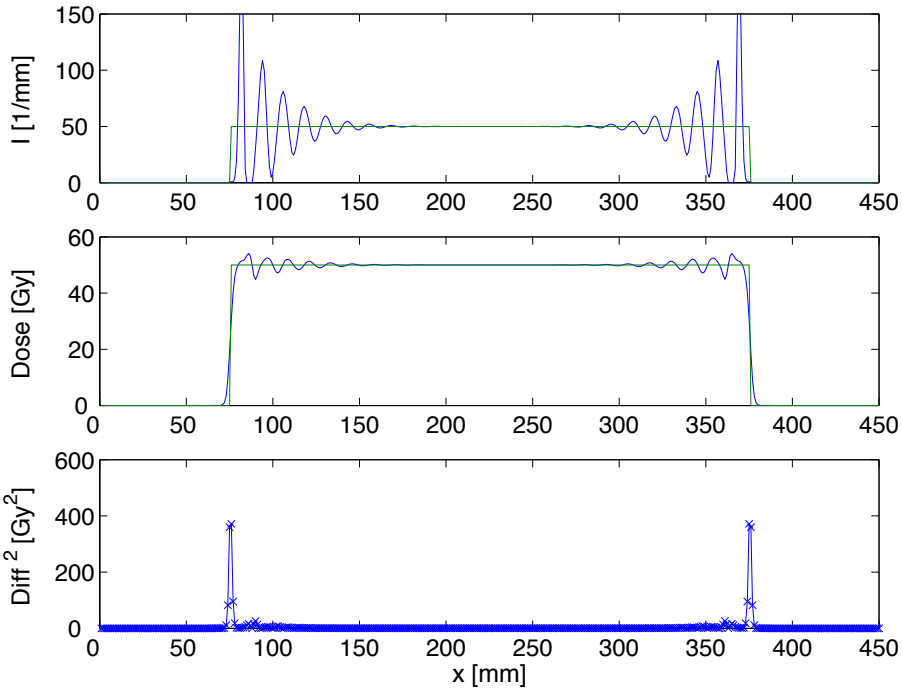

Figure 5.3: Results of a simulation for a block shaped prescription dose profile, with $a = 300$ mm, a Gaussian beam with $\sigma = 8$ mm and an aperture of 13 mm in diameter. Top graph shows intensity (blue) as function of position. First intensity estimate for the iterations is also plotted (green). Center graph shows calculated dose (blue) and prescription dose (green) as function of position. Bottom graph shows squared difference between calculated and prescribed dose.

distribution necessary to achieve this contains considerably more modulation compared to the distribution resulting from the simulation with a 3 mm Gaussian beam. These modulations can be decreased by using an aperture, as can be seen in figure 5.13. From this figure it can also be seen that, when using an aperture, the amount of intensity modulation is still larger than when using a Gaussian beam with $\sigma = 3$ mm.

5.4 Motion compensation

Figure 5.14 shows the calculated dose distributions for a block-shaped prescription dose profile. In this figure, the optimal dose, dose to a moving tumor without compensation and dose to a moving tumor with motion compensation are displayed. The compensated dose distribution is calculated in a moving frame of reference. The dose distribution in a static frame of reference is also displayed. This is the dose distribution that agrees with the compensated distribution delivered to a moving target, if the motion kernel describes the

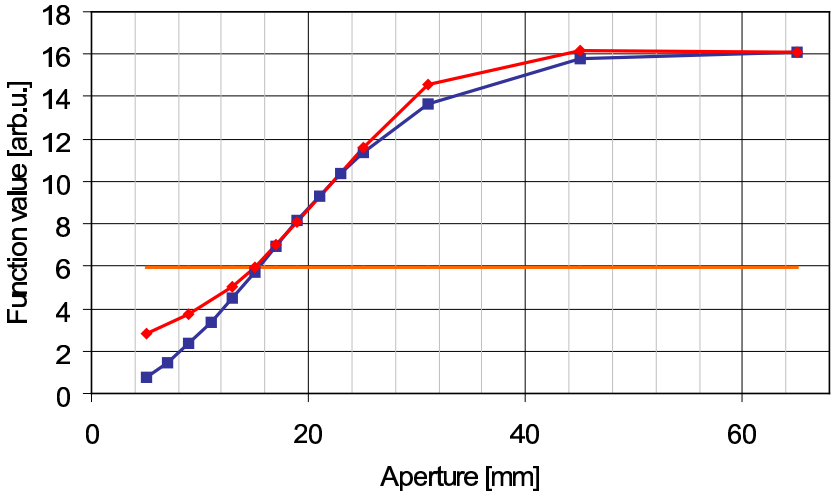

Figure 5.4: Results of simulations for a block shaped prescription dose profile, with $a = 300$ mm. Shown are χ^2 (red) and beam intensity (blue) as function of the aperture width. Maximum intensity is scaled to χ^2 at the maximum aperture width. The value of χ^2 for a Gaussian beam with $\sigma = 3$ mm is also plotted (orange).

actual motion correctly. Calculation showed that, for the described case, target motion would result in an increase of 67% in the value of the objective function (which is the measure of how closely the delivered distribution reproduces the prescription). When the target motion was taken into account in the optimization, by using the motion kernel, the increase in the objective function was 39% compared to a situation without motion.

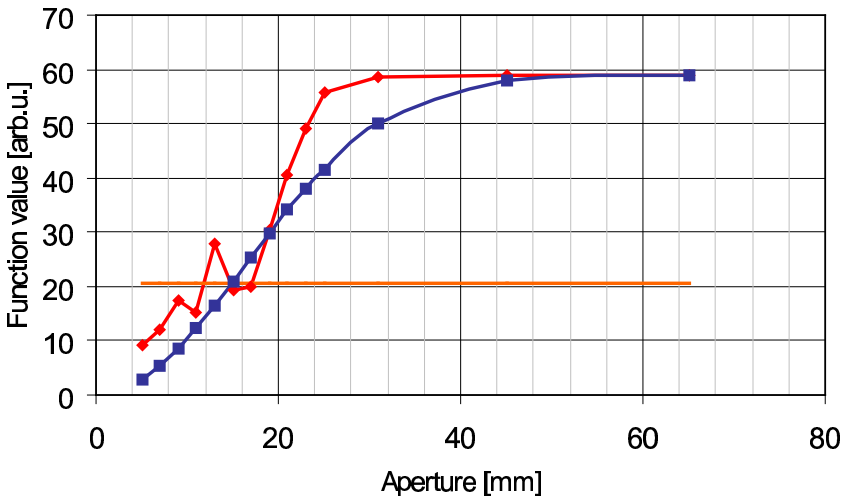

Figure 5.5: Results of simulations for a block shaped prescription dose profile, with $a = 30$ mm. Shown are χ^2 (red) and beam intensity (blue) as function of the aperture width. Maximum intensity is scaled to χ^2 at the maximum aperture width. The value of χ^2 for a Gaussian beam with $\sigma = 3$ mm is also plotted (orange).

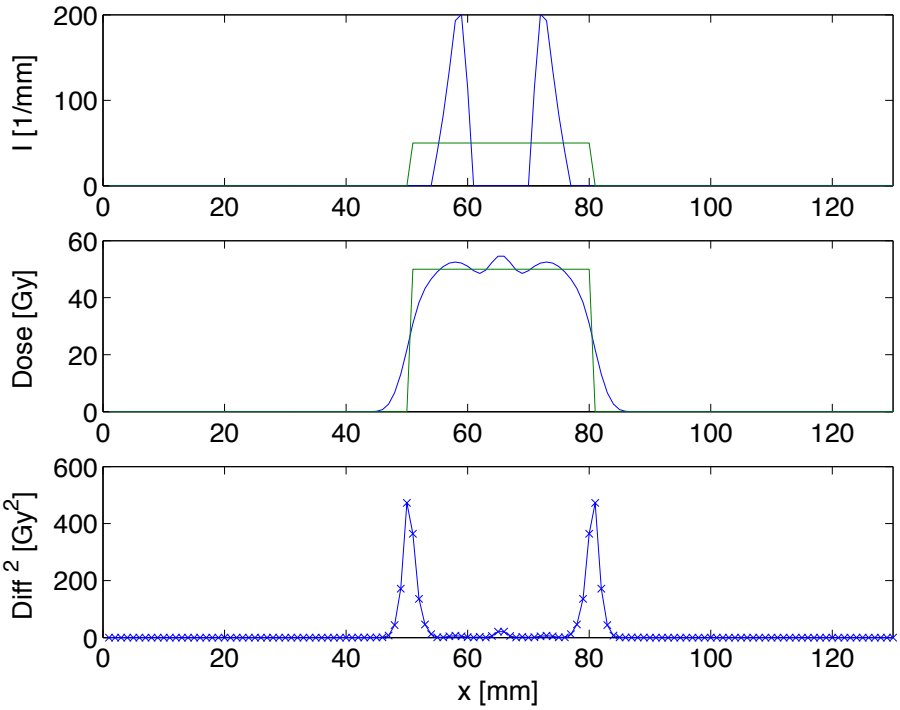

Figure 5.6: Results of a simulation for a block shaped prescription dose profile, with $a = 30$ mm, a Gaussian beam with $\sigma = 8$ mm and an aperture of 17 mm in diameter. Top graph shows intensity (blue) as function of position. First intensity estimate for the iterations is also plotted (green). Center graph shows calculated dose (blue) and prescription dose (green) as function of position. Bottom graph shows squared difference between calculated and prescribed dose.

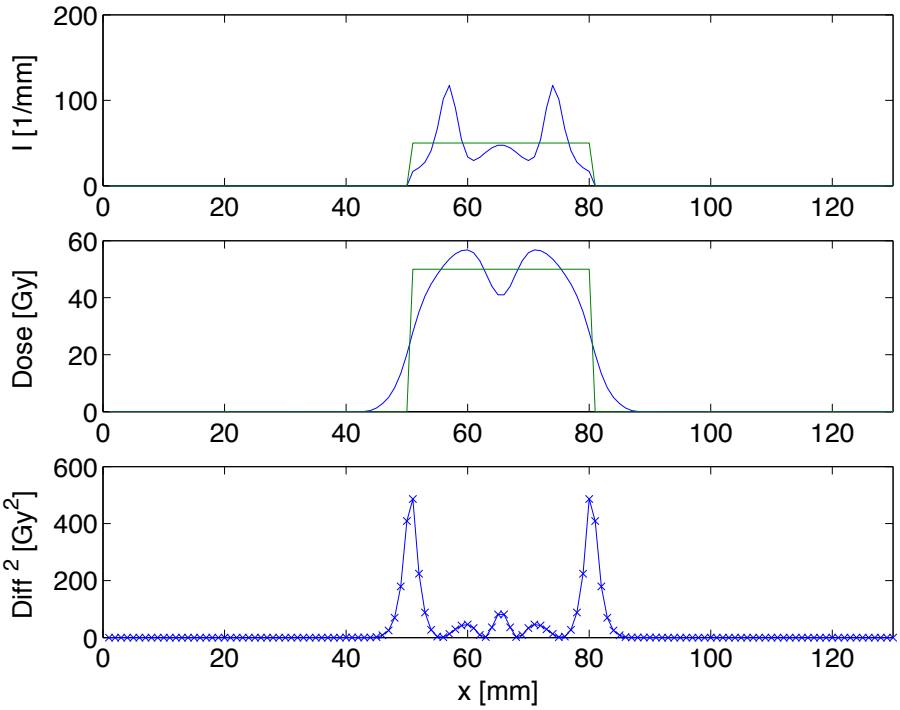

Figure 5.7: Results of a simulation for a block shaped prescription dose profile, with $a = 30$ mm, a Gaussian beam with $\sigma = 8$ mm and an aperture of 13 mm in diameter. Top graph shows intensity (blue) as function of position. First intensity estimate for the iterations is also plotted (green). Center graph shows calculated dose (blue) and prescription dose (green) as function of position. Bottom graph shows squared difference between calculated and prescribed dose.

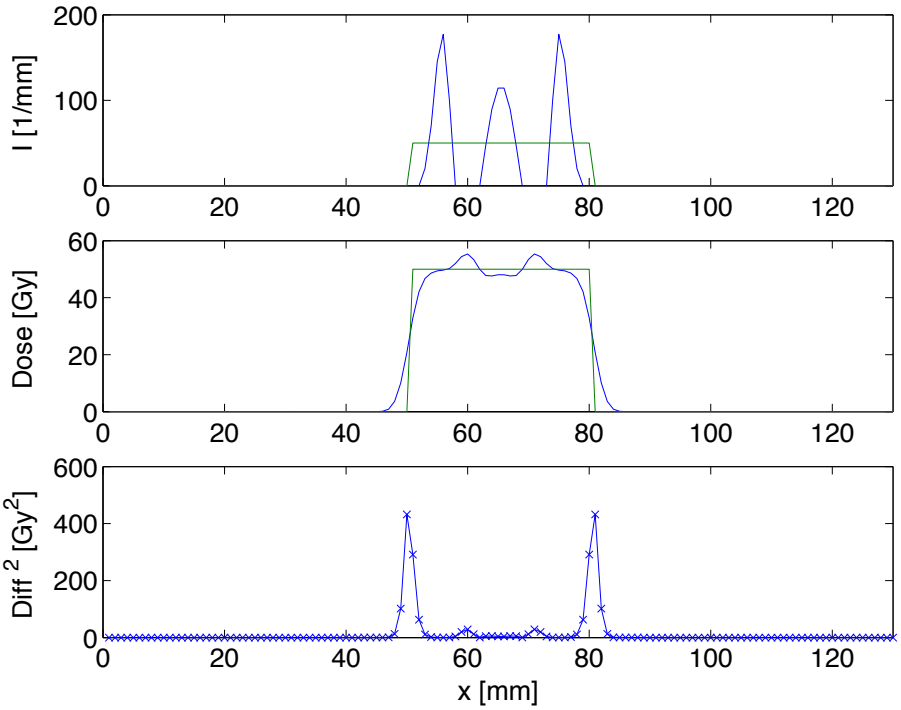

Figure 5.8: Results of a simulation for a block shaped prescription dose profile, with $a = 30$ mm, a Gaussian beam with $\sigma = 8$ mm and an aperture of 11 mm in diameter. Top graph shows intensity (blue) as function of position. First intensity estimate for the iterations is also plotted (green). Center graph shows calculated dose (blue) and prescription dose (green) as function of position. Bottom graph shows squared difference between calculated and prescribed dose.

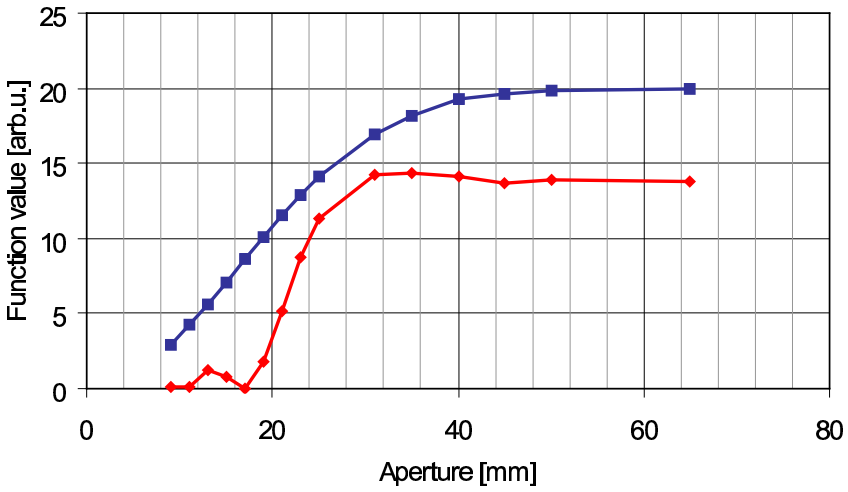

Figure 5.9: Results of simulations for a smooth prescription dose profile, with $a = 30$ mm. Shown are χ^2 (red) and beam intensity (blue) as function of the aperture width. Maximum intensity is scaled to 20 (arb.u.).

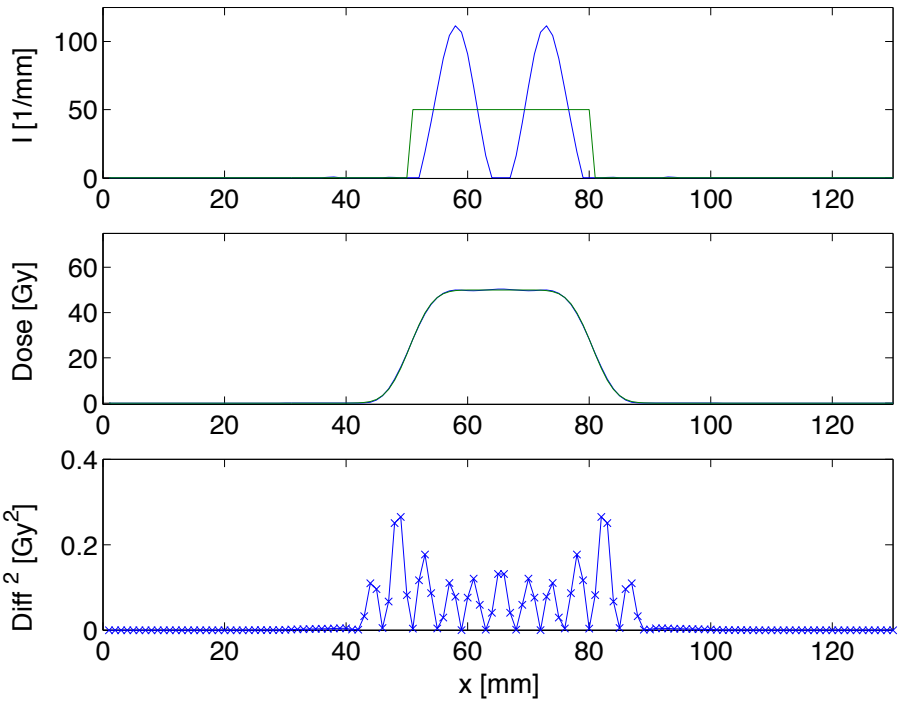

Figure 5.10: Results of a simulation for a smooth prescription dose profile, with $a = 30$ mm, a Gaussian beam with $\sigma = 8$ mm and an aperture of 17 mm in diameter. Top graph shows intensity (blue) as function of position. First intensity estimate for the iterations is also plotted (green). Center graph shows calculated dose (blue) and prescription dose (green) as function of position. Bottom graph shows squared difference between calculated and prescribed dose.

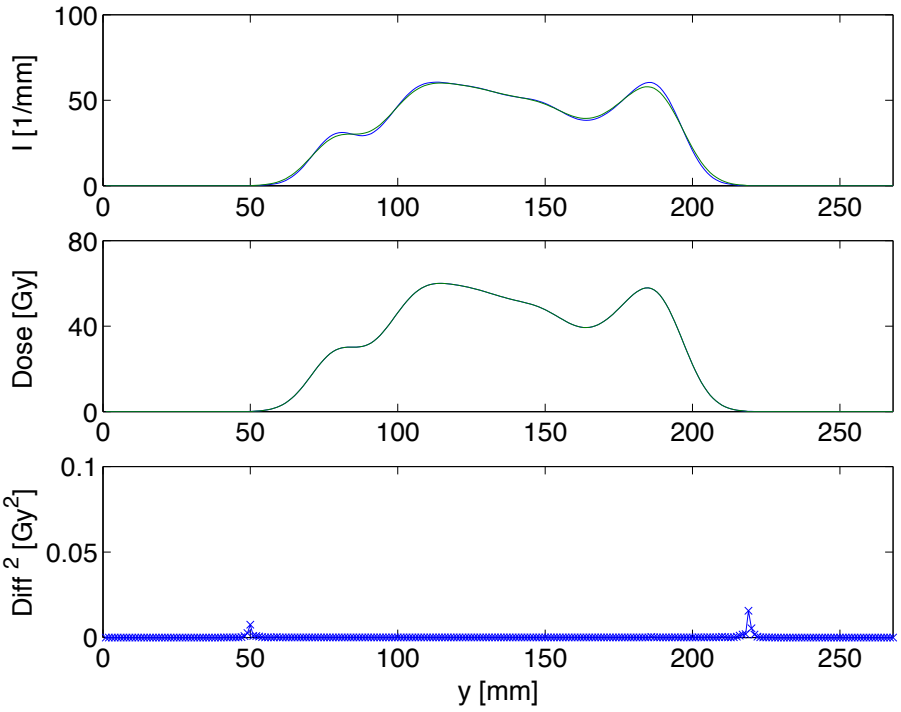

Figure 5.11: Results of a simulation for the clinical case using a Gaussian beam with $\sigma = 3$ mm. Top graph shows intensity (blue) as function of position. First intensity estimate for the iterations is also plotted (green). Center graph shows calculated dose (blue) and prescription dose (green) as function of position. Bottom graph shows squared difference between calculated and prescribed dose.

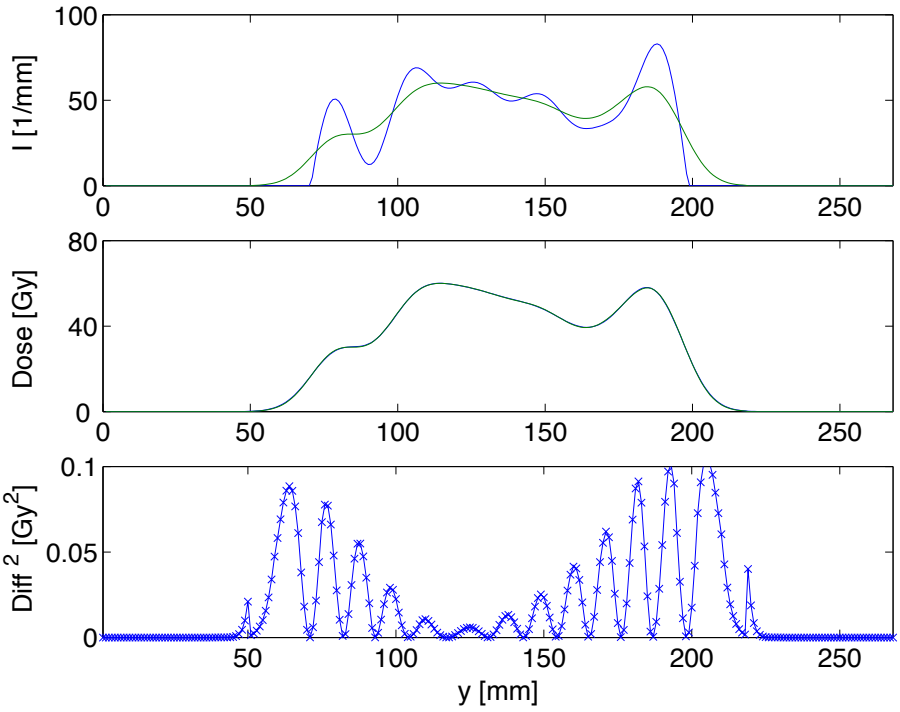

Figure 5.12: Results of a simulation for the clinical case using a Gaussian beam with $\sigma = 8$ mm. Top graph shows intensity (blue) as function of position. First intensity estimate for the iterations is also plotted (green). Center graph shows calculated dose (blue) and prescription dose (green) as function of position. Bottom graph shows squared difference between calculated and prescribed dose.

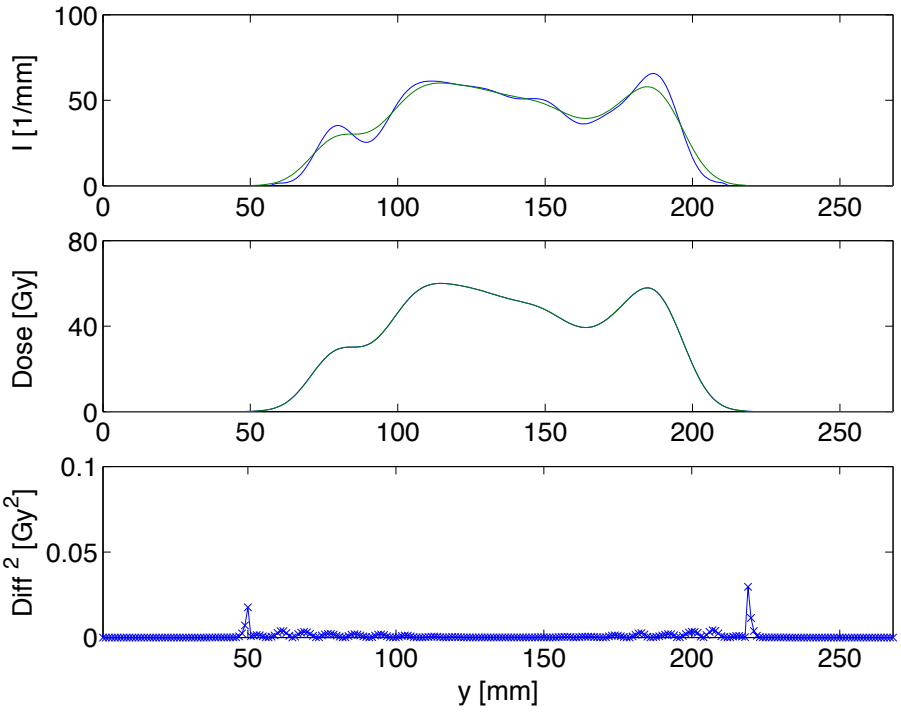

Figure 5.13: Results of a simulation for the clinical case using a Gaussian beam with $\sigma = 8$ mm and an aperture of 19 mm in diameter. Top graph shows intensity (blue) as function of position. First intensity estimate for the iterations is also plotted (green). Center graph shows calculated dose (blue) and prescription dose (green) as function of position. Bottom graph shows squared difference between calculated and prescribed dose.

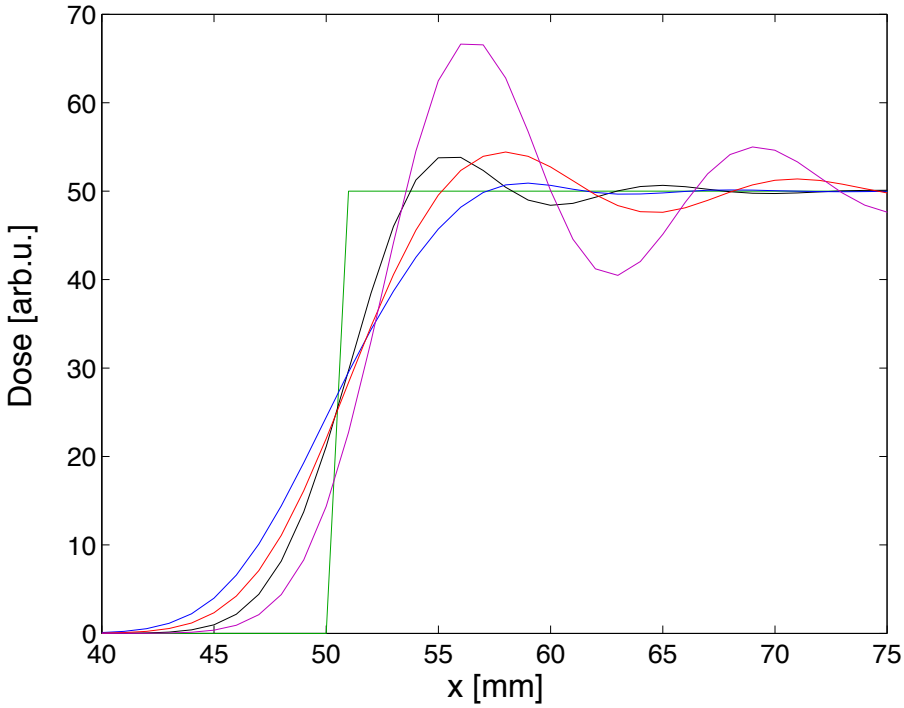

Figure 5.14: Dose distributions resulting from intensity distributions calculated for a static target (black), a moving target without motion compensation (blue) and a moving target with motion compensation (red). Furthermore, the dose distribution that would be obtained by delivering the intensity profile, which was optimized for the moving target, to a static phantom (purple), as well as the dose prescription used in these simulations (green) is shown

Chapter 6

Discussion

6.1 Apertures

Because the aperture diameter required to deliver adequate dose distribution with broad beams is small compared to the beam diameter, a large part of the beam intensity is lost, reducing efficiency substantially. This also results in the additional production of neutrons due to interaction of the protons with aperture material. These neutrons have to be shielded off. The intensity distributions also show a high degree of modulation when using an aperture. In practice, it's difficult or even impossible to deliver such distributions because the rate of change in intensity during scanning is physically limited. The fact that intensity modulations appear at all, even without the use of an aperture, is due to the choice of penalty factors. Because the penalty for overdosage outside the target is chosen to be equal to the penalty for under- and overdosage inside the target, the only way to obtain a large dose gradient is to give a narrow intensity pulse, which has to be compensated for by neighboring low intensity. For narrow prescription doses, modulations in χ^2 as function of aperture width are visible. These are caused by interference between intensity modulations from both sides of the intensity distribution. Because of these modulations in χ^2, the optimal aperture width depends on the target size. As a result of this, it's not possible to use a single aperture diameter for all irradiations. Another problem that arises when using apertures, is the increased difficulty spacing neighboring scan lines, due to the decreased beam penumbra. The error in the dose distribution due to scan line positioning inaccuracies increases with decreasing beam penumbra. This problem was not investigated in this simulation study, because all simulations were done in 1D, using only one scan line. A possible solution to this problem would be the use of a slit aperture, instead of a circular aperture. A slit aperture decreases the beam penumbra in the scanning direction, whilst preserving the original penumbra in the direction perpendicular to the scanning direction, hereby possibly solving or reducing line overlap problems.

6.2 Motion compensation

In a clinical situation, tumor motion is often very irregular. Because the motion at the time of irradiation is not exactly known when planning the treatment, there will be a mismatch between the motion kernel used in the optimization process and the actual target probability distribution function. This mismatch will produce additional errors, which should be studied as well.

Chapter 7

Conclusions

7.1 Apertures

From the simulations, it can be concluded that it is possible to use a broad proton beam in combination with an aperture to deliver equally well dose distributions compared to using a narrow Gaussian proton beam. This delivery method however has certain disadvantages. Because the aperture diameter has to be relatively small compared to the beam diameter, a large part of the intensity will be lost. Besides decreasing efficiency, this will also result in the extra production of neutrons due to interaction of the proton beam with aperture material. These neutrons have to be shielded off. Another disadvantage of using an aperture is the fact that the optimal diameter depends on the prescribed dose. Because of this, it is not possible to use one aperture for all irradiations. When using an aperture, modulations in the intensity map will also increase. This is due to the decreased overlap from neighboring beam elements, resulting from the decreased beam profile penumbra. This effect can result in delivery difficulties. Because of the decreased penumbra of cut off beams compared to Gaussian beams, it's also more important to have the correct distance, in the slow scan direction, between neighboring scan lines. A small error in positioning will have a larger effect on the dose distribution than when using a Gaussian beam.

7.2 Motion compensation

From these simulations it can be concluded that, in an ideal situation, motion compensation in the treatment planning stage can correct a substantial part of the reduced conformality, introduced by target motion. The extent of improvement however, depends on how well the averaged target probability distribution function describes the actual motion. Although the motion compensation seems to work to some extent, the effect of motion irregularities and associated errors should be studied more extensively.

7.3 Outlook

Instead of using an aperture for the complete irradiation, a promising approach could be to deposit the bulk of the dose with a relatively broad beam, and to sharpen the edges and carve fine details with a narrow beam, which could be produced with a small aperture. This could solve part of the efficiency and neutron production problems. It's also recommendable to include gradient limits in the optimization procedure, to account for physical delivery limitations. A suitable optimization algorithm for this has not yet been found. One possible method can be seen in appendix B. The disadvantage of this method is that it uses a gradient constraint, which tries to minimize intensity gradients with a certain pre-set importance, instead of using a (numerical) gradient limit.

To be able to apply motion compensation through the use of motion kernels, it's important to investigate possible errors introduced by this method (e.g. sensitivity to mismatches in kernels). It would also be interesting/usefull to compare the benefits of motion compensation in the treatment planning stage to these of realtime motion compensation.

Bibliography

[Bor90] T. Bortfeld, *Neue Methoden zur Lösung des inversen Problems der Strahlentherapieplanung* (PhD thesis, Ruprechts-Karls Universät Heidelberg, Germany, 1990)

[Boy02] A.L. Boyer, M. Goitein, A.J. Lomax and E.S. Pedroni, *Radiation in the Treatment of Cancer* (Physics Today, September 2002)

[Goi02] M. Goitein, A.J. Lomax and E.S. Pedroni, *Treating Cancer With Protons* (Physics Today, September 2002)

[Lom99] A.J. Lomax, *Intensity modulation methods for proton radiotherapy* (Phys. Med. Biol., Vol. 44, 1999, pg 185-205)

[Nil01] S. Nill, *Development and application of a multi-modality inverse treatment planning system* (PhD thesis, Ruperto-Carola University of Heidelberg, Germany, 2001)

[Ped95] E. Pedroni, R. Bacher, H. Blattmann, T. Böhringer, A. Coray, A. Lomax, S. Lin, G. Munkel, S. Scheib, U. Schneider and A. Tourovsky, *The 200-MeV proton therapy project at the Paul Scherrer Institute: conceptual design and practical realization* (Med. Phys., Vol. 22, No. 1, January 1995, pg 37-53)

[Web97] S. Webb, *The Physics of Conformal Radiotherapy, Advances in Technology* (IOP Publishing Ltd, 1997)

[Web98] S. Webb, *Inverse planning with constraints to generate smoothed intensity-modulated beams* (Phys. Med. Biol., Vol. 43, 1998, pg 2785-2794)

Appendix A

Motion kernel

The motion of a tumor is approximated by a sine function, and is thus given by

$$x(t) = A\sin(t), \tag{A.1}$$

with $x(t)$ the position at time t and A the amplitude of motion. The velocity of motion is then given by

$$v(t) = \frac{dx}{dt} = A\cos(t) = A\sqrt{1-\sin^2(t)}. \tag{A.2}$$

Changing the variable from t to x in A.1 gives

$$t(x) = \arcsin(\frac{x}{A}). \tag{A.3}$$

Substitution of A.3 in A.2 gives

$$v(x) = A\sqrt{1-\sin^2(\arcsin(\frac{x}{A}))} = A\sqrt{1-\frac{x^2}{A^2}}. \tag{A.4}$$

From this, the position probability distribution can be found by

$$P(x) \sim \frac{1}{v(x)} = \frac{1}{A\sqrt{1-\frac{x^2}{A^2}}}. \tag{A.5}$$

Appendix B

Tikhonov optimization

A second optimization method used in this study is called the Tikhonov method, used with a gradient descent algorithm. This method incorporates a gradient constraint and is defined by

$$\hat{f} = \underset{f>0}{\operatorname{argmin}} \|w(p - Bf)\|_2^2 + \lambda \|\nabla f\|_2^2 \tag{B.1}$$

where $\hat{f}$ is the optimum intensity pattern f, for a certain dose prescription p, beam matrix B, penalty vector w and relative gradient constraint importance λ.

The intensity of a beam is always positive. To incorporate this positivity constraint, the intensity f_i is defined by $f_i = h_i^2$ and the optimization problem becomes

$$\hat{h} = \underset{h}{\operatorname{argmin}} J(h), \tag{B.2}$$

where

$$J(h) = \|p - B(h \odot h)\|_2^2 + \lambda \|D(h \odot h)\|_2^2, \tag{B.3}$$

with D the difference matrix and $\odot$ representing an element-by-element vector product.

The optimization is done by a steepest descent algorithm, defined by

$$\hat{h}^{(n+1)} = \hat{h}^{(n)} + \alpha^{(n)} d^{(n)}, \tag{B.4}$$

where $d^{(n)}$ is the gradient, given by

$$d^{(n)} = \nabla_h J(\hat{h}^{(n)}) = \frac{dJ}{dh} = \frac{df}{dh} \cdot \frac{dJ}{df} = \operatorname{diag}(2h) \cdot \left[(B^T B + D^T D) f - B^T p \right], \tag{B.5}$$

and $\alpha^{(n)}$ is the step size, given by

$$\alpha^{(n)} = \underset{\alpha}{\operatorname{argmin}} J(\hat{h}^{(n)} + \alpha^{(n)} d^{(n)}). \tag{B.6}$$

Acknowledgements

I would like to thank Thomas Bortfeld, PhD for giving me the opportunity to fulfill my internship at MGH and for guiding and advising me wherever possible, Alexei Trofimov, PhD for all the time and effort he put into guiding me through the field of radiation therapy, John Wolfgang, PhD for his help concerning Linux in specific, and computers in general, Eike Rietzel, PhD for supplying me with data for the motion compensation research and for all of our stimulating conversations, and the rest of the MGH team (Harald, Steve, Ross, Greg, Toni, Lily, Hanne and George) for making my time in Boston as pleasant as possible

Furthermore, I would like to thank Profs. Eric Miller and Dana Brooks of Northeastern University for their help in finding suitable optimization algorithms.

I would also like to thank the 'Koningin Wilhelmina Fonds' and the Eindhoven University of Technology for their financial contributions, making my internship possible.

Furthermore, I would like to thank my family and friends for their support, and in special my parents for supporting me both mentally and financially.

Last but not least, I would like to thank ir. Herman van Kleffens for finding a suitable internship position and for his guidance during my stay in Boston.